Equivalent Current Method for Bistatic Scattering at a Circular Edge

K.W. Kark [1])

Abstract An efficient analysis is presented for calculating the far zone fields scattered by a perfectly-conducting, open-ended, semi-infinite circular waveguide which is excited by an external electromagnetic plane wave. The geometrical theory of diffraction (GTD) is employed to derive electric and magnetic equivalent line currents along the circular edge of the aperture of the waveguide. The line current distribution is approximately taken as an equivalent for the circular edge, bounding the aperture of the cylinder. The radiation behaviour of the calculated line currents is found via an integral representation of the field equations. For the bistatic diffraction integrals new approximate solutions could be found. Three-dimensional directional patterns show the polarization dependent scattering characteristics via a representation of the spatial distribution of the radial energy-flux density.

1. Introduction

This paper considers the radar problem of bistatic scattering of plane electromagnetic waves at a semi-infinite circular cylinder. The diffraction at the circular rim of the aperture is treated in detail. Structures of circular shape which are used for reflector antennas, jet air intakes and satellites are important components for the analysis of complicated bodies using the geometrical theory of diffraction (GTD). Hitherto existing ray-optical investigations only deal with the monostatic backscattering from a circular aperture rim (*Pathak et al* [10]). In the following analytical approximate solutions for the diffraction integrals which appear in a bistatic scattering environment are given for the first time. The integrals are derived via the equivalent current method (ECM). To that end the ray-optical approximation of the geometrical theory of diffraction is used. Thus a very compact representation of the scattered field could be found which is much better suited for numerical computations than the exact field solution derived by the Wiener-Hopf-method (*Johnson* und *Moffatt* [3]).

2. The incident wave

The direction of incidence of the plane wave is restricted to a meridional domain of $0° \le \vartheta_i \le 70°$; accordingly only scattering directions are looked at which are located in the same interval $0° \le \vartheta_s \le 70°$. For this geometrical arrangement of source and receiver it seams natural to neglect the surface currents on the outer and inner cylindrical surfaces since the dominant scattering contribution arises from the diffration at the circular rim of the aperture (Figure 1). The center point of the circular aperture defines the origin of a spherical coordinate system in which the incident plane wave and the scattered field are described.

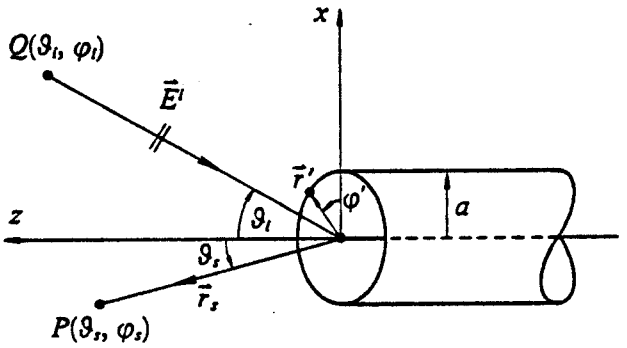

Figure 1. Bistatic scattering at a semi-infinite circular cylinder. The source Q and the sink P are located in far zone of the circular rim of the aperture. The allowable angle domain of the following approximate computations is about $0° \le \vartheta_i, \vartheta_s \le 70°$.

To represent the incident wave at an arbitrary point $P(\vec{r})$ following ansatz is made which uses the wave vector[2]) $\vec{k}_i = -k_0 \hat{r}_i$ for harmonic time dependence ($e^{j\omega t}$):

$$\vec{E}^i = \left(A^i_\vartheta \hat{\vartheta}_i + A^i_\varphi \hat{\varphi}_i \right) e^{-j \vec{k}_i \cdot \vec{r}}$$
$$\vec{H}^i = Y_0 \vec{E}^i \times \hat{r}_i \quad . \tag{1}$$

The wave number is $k_0 = \omega\sqrt{\mu_0 \varepsilon_0}$ and $Z_0 = 1/Y_0 = \sqrt{\mu_0/\varepsilon_0}$ is the characteristic impedance of the free space. A^i_ϑ and A^i_φ are complex phasors; they determine the polarization properties of the incident plane wave. Using $\vec{r} = r\hat{r}$ the propagation term in Eq. (1) can be re-written:

$$e^{-j \vec{k}_i \cdot \vec{r}} = e^{j k_0 r \, \hat{r}_i \cdot \hat{r}} \quad ,$$

with

$$\hat{r}_i \cdot \hat{r} = \sin\vartheta_i \sin\vartheta \cos(\varphi - \varphi_i) + \cos\vartheta_i \cos\vartheta \, . \tag{2}$$

In the following only the azimuthal angle of incidence $\varphi_i = 0°$ is considered; this means no restriction since the scattering arrangement is rotationally symmetrical around the z-axis. The plane of incidence which is formed by the wave vector $\vec{k}_i = -k_0 \hat{r}_i$ and the z-axis is thus identical to the x-z-plane of the spherical coordinate system (Figure 1). In the special case of $\varphi_i = 0°$ a horizontally polarized (H) incident plane wave is obtained for $A^i_\vartheta = 0$; for $A^i_\varphi = 0$ vertical polarization (V) occurs. The sense of circular polarization is

---

[1]) Dr. Klaus W. Kark, Institut für Hochfrequenztechnik, Deutsche Forschungs- und Versuchsanstalt für Luft- und Raumfahrt, DFVLR Oberpfaffenhofen, D-8031 Wessling / Obb., F.R. Germany.

[2]) In this paper vectors are indicated by an arrow (→) and unit vectors by a hat (^).

called right handed (RHC) or left handed (LHC) if the direction of rotation is clockwise or counterclockwise for an observer looking in the direction of propagation.

3. Derivation of the diffraction integrals

Ray-optical methods cannot be used for field computations near or on caustics which appear in connection with circular edges. A caustic is a focal line; every caustic point is crossed by an infinite set of rays accordingly to the principles of the geometrical theory of diffraction. Thus the total ray field leads to a singularity and the method fails. For normal incidence ($\vartheta_i = 0°$) the whole z-axis of the circular cylinder is a caustic. In general integral representations of the field equations can be applied to compute the field in such regions. To that end equivalent electric and magnetic line currents (I_e and I_m) are introduced which flow along the diffracting edge (*Knott* und *Senior* [6]). These currents are taken as an equivalent for the diffracting edge. Their radiation behaviour in the free space, i.e. after having removed the cylinder, is considered in the following. Maxwell's equations for harmonic time dependence ($e^{j\omega t}$) and homogeneous isotropic domains are dealt with:

$$\begin{aligned} \nabla \times \vec{H} &= j\omega \varepsilon_0 \vec{E} + \vec{J} \\ \nabla \times \vec{E} &= -j\omega \mu_0 \vec{H} - \vec{M} \quad . \end{aligned} \tag{3}$$

$\vec{J}$ and $\vec{M}$ denote the superposition of localized and induced electric and magnetic current densities. They represent the sources of the incident and the scattered field:

$$\vec{J} = \vec{J}_e + \vec{J}_i \quad , \qquad \vec{M} = \vec{M}_e + \vec{M}_i \quad .$$

The source current densities $\vec{J}_i$ and $\vec{M}_i$ may be expressed via the line currents I_e and I_m which are induced along the circular rim of the aperture of the cylinder. Their representation in spherical coordinates at a point $\vec{r}' = a\,\hat{\rho}' = a\,(\hat{x}\cos\varphi' + \hat{y}\sin\varphi')$ on the circular edge is:

$$\begin{aligned} \vec{J}_i(\vec{r}') &= I_e(\varphi')\,\frac{1}{r'}\,\delta(r'-a)\,\delta(\vartheta'-\frac{\pi}{2})\,\hat{\varphi}' \\ \vec{M}_i(\vec{r}') &= I_m(\varphi')\,\frac{1}{r'}\,\delta(r'-a)\,\delta(\vartheta'-\frac{\pi}{2})\,\hat{\varphi}' \quad . \end{aligned} \tag{4}$$

Dirac's delta function is denoted by δ. Approximate values for the line currents I_e and I_m will be given in section 3.2.

The total field is composed of the incident wave and the scattered field:

$$\begin{aligned} \vec{E} &= \vec{E}^i + \vec{E}^s \\ \vec{H} &= \vec{H}^i + \vec{H}^s \quad . \end{aligned}$$

The incident plane wave is given in Eq. (1). The differential equation system (3) can be transformed into an integral form (see e.g. *Schroth* and *Stein* [13]); thus one obtains the solution for the scattered field in the Fraunhofer far field region:

$$\vec{E}^s(\vec{r}_s) = jk_0 a\,\frac{e^{-jk_0 r_s}}{4\pi r_s}\int_0^{2\pi}\left[Z_0\,\hat{r}_s\times(\hat{r}_s\times\hat{\varphi}')\,I_e(\varphi') + \hat{r}_s\times\hat{\varphi}'\,I_m(\varphi')\right]e^{jk_0\hat{r}_s\cdot\vec{r}'}\,d\varphi' \tag{5}$$

$$\vec{H}^s(\vec{r}_s) = Y_0\,\hat{r}_s\times\vec{E}^s(\vec{r}_s) \quad . \tag{6}$$

The current densities $\vec{J}_i$ and $\vec{M}_i$ have already been inserted from Eq. (4). The integration path and the mutual location of the integration point and the field point P is shown in Figure 2. The standard far zone approximations

$$k_0 R_s \gg 1 \quad , \qquad r_s \gg r' = a$$

are applied. R_s ist the distance between the diffraction point on the rim and the considered field point (*Silver* [15]):

$$R_s \approx r_s - \hat{r}_s\cdot\vec{r}' = r_s - a\,\sin\vartheta_s\,\cos\,(\varphi' - \varphi_s) \quad . \tag{7}$$

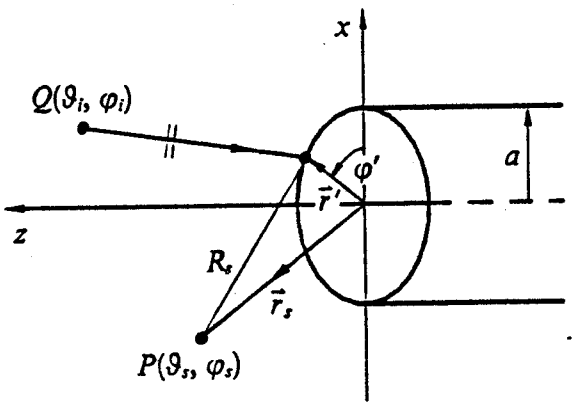

Figure 2. The integration path. The diffraction point at $\vec{r}' = a\,\hat{\rho}'$ is part of the integration path along the circular rim.

For a clearer subsequent derivation of the edge currents I_e and I_m some basic ideas regarding the diffraction at a half-plane are presented first.

3.1 The law of edge diffraction

The curved circular edge of a semi-infinite waveguide can locally be modeled by a half-plane tangent to the edge at the diffraction point. Using a ray-optical approach (*geometrical theory of diffraction* - GTD, see *Kouyoumjian et al* [9]) the edge diffracted field can be computed approximately. The relation between the incident and diffracted ray is described via an edge-diffraction coefficient which depends on frequency, polarization, incidence and diffraction angle.

The local edge angles of the incident (β_i, ψ_i) and the diffracted ray (β_s, ψ_s) (see Figure 3) are connected via simple trigonometric relations with the global directions of incidence and scattering (ϑ_i, φ_i; ϑ_s, φ_s) (see Figure 1 and Figure 2). The angles are restricted to the range $0 \le \beta_{i,s} \le \pi$ and $0 \le \psi_{i,s} \le 2\pi$. The law of edge diffraction which is based on the extended Fermat's principle (*Keller* [5]) reads:

$$\beta_s = \beta_i \quad .$$

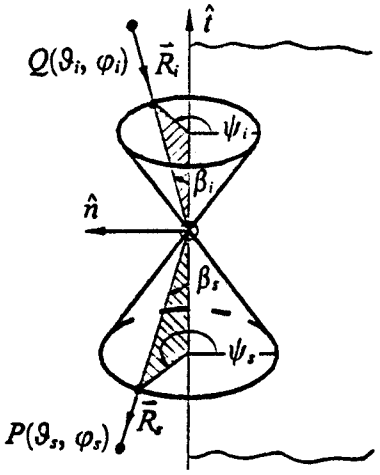

Figure 3. **The ray-fixed coordinate system. The angles $\beta_{i,s}$ and $\psi_{i,s}$ for incident and diffracted ray are defined relative to the tangent $\hat{t}$ and the normal $\hat{n}$ of the edge of the half-plane. The hatched areas denote the plane of incidence and the plane of diffraction.**

Each ray which hits the edge excites a cone of diffracted rays. For normal incidence ($\vartheta_i = 0° \rightarrow \beta_i = \pi/2$) the cone degenerates to a circular disc. The diffracted field can only be computed in certain directions of space lying on the Keller cone.

The GTD - edge diffraction coefficients for the half-plane are defined as follows:

$$D_{e,m} = -\frac{e^{-j\pi/4}\sqrt{\lambda_0}}{4\pi\sqrt{\sin\beta_i \sin\beta_s}} \times \times \left[\frac{1}{\cos\frac{\psi_i - \psi_s}{2}} \mp \frac{1}{\cos\frac{\psi_i + \psi_s}{2}} \right] . \quad (8)$$

The $-$ signs describes the electric case (D_e) and the $+$ sign the magnetic one (D_m). The wavelength $\lambda_0 = 2\pi/k_0$ is related to the wave number. For $\beta_s = \beta_i$ Eq. (8) gives the ordinary GTD edge diffraction coefficients. A heuristic argumentation allows the approximate use of the same expression also for scattering directions which do not lie on the cone of diffracted rays ($\beta_s \neq \beta_i$). The symmetry of the square root term in Eq. (8) guarantees the reciprocity when interchanging the incident with the diffracted ray and has proved its applicability in numerical comparisons (*Knott* and *Senior* [7]). For later purposes the always real modified diffraction coefficients are defined as follows:

$$\delta_{e,m} = k_0 a\, e^{j\pi/4} \frac{D_{e,m}/\sqrt{\lambda_0}}{\sqrt{\sin\beta_i \sin\beta_s}} . \quad (9)$$

The GTD edge diffraction coefficients become singular at the zeros of the cosine functions in Eq. (8). These singularities are exactly located on the shadow and the reflection boundary of the incident wave relative to the diffracting edge. While crossing these boundaries the direct or the reflected ray suddenly disappears. The location of the incident shadow boundary - ISB and the reflection shadow boundary - RSB can be described via the local edge angles (see Figure 3):

$$\psi_s^{ISB} = \pi + \psi_i , \quad \psi_s^{RSB} = \pi - \psi_i . \quad (10)$$

The discussed singularities and their surrounding transition regions are the reasons that only a global angle domain of about $0° \leq \vartheta_{i,s} \leq 70°$ can be considered. The geometrical theory of diffraction can be enlarged by higher order terms. Doing this leads to new diffraction coefficients from which fields can be derived which have no singular behaviour while crossing the shadow and the reflection boundaries. This uniform geometrical theory of diffraction - UTD (*Kouyoumjian* and *Pathak* [8]) possesses the same disadvantage, just as the GTD, that the field representation becomes singular at caustics. By the aid of an integral representation of the field equations, approximations for the fields can be obtained also in caustic regions using equivalent line currents on the circular edge of the aperture.

3.2 Equivalent edge currents

To avoid the caustic problem of GTD and UTD the equivalent current method - ECM (see e.g. *Pathak* [12]) is used. To that end, an integral representation of the field equations, just as has already been given in the Eqs. (5) and (6), is needed. The ECM can of course determine the scattered field even outside caustic regions; the computed values in those regions agree asymptoticly with the field values which can also be found there using the GTD.

The equivalent edge currents are determined from the incident field via the GTD - edge diffraction coefficients for the half-plane (see Eq. (8)). This is possible since the edge is located far away from the caustic region. The so computed line currents are no physical currents; it is not possible to derive from them the scattered field for all directions of space. The heuristic extension of the region of applicability for the GTD - edge diffraction coeficients to all spatial directions even away from the cone of diffracted rays (see Figure 3) allows an approximate field computation in the whole interesting meridional angle domain $0° \leq \vartheta_i, \vartheta_s \leq 70°$. The computed ECM fields show the same singularities at shadow or reflection boundaries (ISB, RSB, see Eq. (10)) just as those fields would do which were derived by a GTD based algorithm.

The equivalent edge currents are derived from those components of the incident field which are locally tangential to the edge using the GTD - edge diffraction coefficients for the half-plane (*Pathak et al* [11]):

$$I_e(\varphi') = -2Y_0\, e^{-j\frac{\pi}{4}}\sqrt{\lambda_0}\, \frac{D_e(\beta_i, \psi_i; \beta_s, \psi_s)}{\sqrt{\sin\beta_i \sin\beta_s}} (\vec{E}^i \cdot \hat{\varphi}')$$
$$I_m(\varphi') = -2Z_0\, e^{-j\frac{\pi}{4}}\sqrt{\lambda_0}\, \frac{D_m(\beta_i, \psi_i; \beta_s, \psi_s)}{\sqrt{\sin\beta_i \sin\beta_s}} (\vec{H}^i \cdot \hat{\varphi}') . \quad (11)$$

The incident field can be found in Eq. (1) and the diffraction coefficients are given in Eq. (8). It is obvious that the equivalent edge currents cannot be real physical currents, since their values depend on the direction of observation ($\vartheta_s, \varphi_s \rightarrow \beta_s, \psi_s$).

Accordingly to the GTD - edge diffraction coefficients the current representation was heuristicly extended to spatial directions away from the diffraction cone ($\beta_s \neq \beta_i$).

The tangential fields at the circular ring $\vec{r}' = a\,\hat{r}' = a\,(\hat{x}\cos\varphi' + \hat{y}\sin\varphi')$ which are needed for the evaluation of Eq. (11) are given below:

$$\vec{E}^i \cdot \hat{\varphi}' = \left[-A_\vartheta^i \cos\vartheta_i \sin(\varphi' - \varphi_i) + A_\varphi^i \cos(\varphi' - \varphi_i) \right] e^{j k_0 a \hat{r}_i \cdot \hat{r}'} \quad (12)$$

$$\vec{H}^i \cdot \hat{\varphi}' = -Y_0 \left[A_\varphi^i \cos\vartheta_i \sin(\varphi' - \varphi_i) + A_\vartheta^i \cos(\varphi' - \varphi_i) \right] e^{j k_0 a \hat{r}_i \cdot \hat{r}'} \quad (13)$$

Starting from the integral representations (5) and (6) one finds the electric and magnetic field components of the scattered field in $\hat{\vartheta}_s$- and $\hat{\varphi}_s$ -direction using the Eqs. (11) to (13):

$$E_\vartheta^s(\vec{r}_s) = f(r_s) \left[I_e^{ss} A_\vartheta^i \cos\vartheta_i \cos\vartheta_s - I_e^{cs} A_\varphi^i \cos\vartheta_s - I_m^{sc} A_\varphi^i \cos\vartheta_i - I_m^{cc} A_\vartheta^i \right] \quad (14)$$

$$H_\varphi^s(\vec{r}_s) = Y_0 E_\vartheta^s(\vec{r}_s)$$

$$E_\varphi^s(\vec{r}_s) = f(r_s) \left[-I_m^{ss} A_\varphi^i \cos\vartheta_i \cos\vartheta_s - I_m^{cs} A_\vartheta^i \cos\vartheta_s - I_e^{sc} A_\vartheta^i \cos\vartheta_i + I_e^{cc} A_\varphi^i \right] \quad (15)$$

$$H_\vartheta^s(\vec{r}_s) = -Y_0 E_\varphi^s(\vec{r}_s) \; .$$

The propagation term of the scattered field which is considered as a plane wave in the far-zone is:

$$f(r_s) = \frac{1}{k_0 r_s} e^{-j k_0 r_s} \; .$$

All eight appearing diffraction integrals $I_{e,m}^{s,c;s,c}$ have the general form:

$$I(k_0 a; \vartheta_i, \varphi_i; \vartheta_s, \varphi_s) = \int_0^{2\pi} h(\varphi') e^{j k_0 a g(\varphi')} d\varphi' \quad , \quad (16)$$

with:

$$g(\varphi') = (\hat{r}_i + \hat{r}_s) \cdot \hat{r}' = \sin\vartheta_i \cos(\varphi' - \varphi_i) + \sin\vartheta_s \cos(\varphi' - \varphi_s) \; ; \quad (17)$$

their subsequent computation is one main part of this work. The diffraction functions $h(\varphi')$ may take eight different forms. The indices e and m or s and c are correponding with the indices of the diffraction integrals in the Eqs. (14) and (15).

$$h_{e,m}^{ss}(\varphi') = \delta_{e,m}(\varphi') \sin(\varphi' - \varphi_i) \sin(\varphi' - \varphi_s)$$
$$h_{e,m}^{cs}(\varphi') = \delta_{e,m}(\varphi') \cos(\varphi' - \varphi_i) \sin(\varphi' - \varphi_s)$$
$$h_{e,m}^{sc}(\varphi') = \delta_{e,m}(\varphi') \sin(\varphi' - \varphi_i) \cos(\varphi' - \varphi_s)$$
$$h_{e,m}^{cc}(\varphi') = \delta_{e,m}(\varphi') \cos(\varphi' - \varphi_i) \cos(\varphi' - \varphi_s)$$

For practical reasons the diffraction functions are subdivided as follows:

$$h(\varphi') = \delta_{e,m}(\varphi')\, T(\varphi')$$

with the trigonometric products

$$T(\varphi') = \begin{Bmatrix} \sin(\varphi' - \varphi_i) \\ \cos(\varphi' - \varphi_i) \end{Bmatrix} \begin{Bmatrix} \sin(\varphi' - \varphi_s) \\ \cos(\varphi' - \varphi_s) \end{Bmatrix} \; .$$

Because of the complicated dependence of the modified diffraction coefficients $\delta_{e,m}$ on the variable of integration φ' the eight diffraction integrals I from Eq. (16) cannot be computed rigorously. The next chapter therefore shows how to construct approximate solutions of these integrals which shall be applicable in the whole interesting range of aspect angles $0° \leq \vartheta_{i,s} \leq 70°$.

4. Approximate solution of the diffraction integrals

The diffraction integrals (16) can be computed numerically. But for a larger waveguide radius ($k_0 a \gg 1$) this approach is very time consuming because of the rapidly oscillating behaviour of the integrand; it is much more economical to use an analytical approximate solution which will be developed in this chapter. It's high accuracy has been proved by comparison with a numerical quadratur.

4.1 The method of stationary phase

To prepare the following uniform integral evaluations this section gives some introductions to the method of stationary phase (see e.g. *James* [2]) for the asymptotic computation of integrals of the type:

$$I = \int_0^{2\pi} h(\varphi') e^{j k_0 a g(\varphi')} d\varphi' \quad , \quad (18)$$

which frequently appear in diffraction theory. If the condition $k_0 a \gg 1$ is met, while $g(\varphi')$ is of order of unity, then the exponential term in the integrand is a rapidly oscillating function of φ' with the exception of certain regions around some so-called stationary points of first order at φ_0', which obey the condition:

$$g'(\varphi_0') = 0 \quad \text{with} \quad g''(\varphi_0') \neq 0 \; .$$

The actual diffraction problem with the function $g(\varphi')$ from Eq. (17) yields the stationary points:

$$\varphi_0' = p\pi + \arctan \frac{\sin\vartheta_i \sin\varphi_i + \sin\vartheta_s \sin\varphi_s}{\sin\vartheta_i \cos\varphi_i + \sin\vartheta_s \cos\varphi_s} \quad . \quad (19)$$

With the supplementary condition $g''(\varphi_0') \neq 0$ there are always two stationary points on the circular aperture rim which lie diametrically on opposite sides of the circle. They define local scattering centres of the circular edge which must be taken into account for a GTD - ray construction as edge diffraction points of singly diffracted rays.

The value of the integral I is dominated by regions around stationary points, if $h(\varphi')$ is only weakly changing in the neighbourhood of φ_0', since the contributions to the integral which result from more distant integration points cancel each other. One finally gets as the aymptotic integral approximation

accordingly to the method of stationary phase (*Erdélyi* [1]):

$$I \approx \sqrt{\frac{2\pi}{k_0 a |g''(\varphi_0')|}}\, h(\varphi_0')\, e^{j\left(k_0 a\, g(\varphi_0') \pm \frac{\pi}{4}\right)} .$$

The + sign is valid for $g''(\varphi_0') > 0$ and the − sign for $g''(\varphi_0') < 0$.

4.2 Uniform integral evaluation

In the following the approximate solution of the eight occuring diffraction integrals with the type

$$I_{e,m}^{s,c;s,c} = \int_0^{2\pi} \delta_{e,m}(\varphi')\, T(\varphi')\, e^{j k_0 a\, g(\varphi')}\, d\varphi' \qquad (20)$$

will be discussed. The idea for an asymptotic representation of the diffraction integrals arises from *Pathak et al* [10] who considered the monostatic special case of radar backscattering from the semi-infinite circular cylinder. This paper gives a generalization of that approach to bistatic scattering. As was shown by *Kark* [4], an approximate solution of the diffraction integrals can be found which is applicable in the whole interesting angle domain of $0° \le \vartheta_{i,s} \le 70°$ and which also in the caustic region yields well defined results:

$$I_{e,m}^{s,c;s,c} \approx \delta_{e,m}(\varphi_0') \int_0^{2\pi} T(\varphi')\, e^{j k_0 a\, g(\varphi')}\, d\varphi' . \qquad (21)$$

The diffraction coefficients $\delta_{e,m}(\varphi_0')$ at the stationary point (19) are obtained from the representation (9).

For the following rigorous computation of the remaining integral in Eq. (21) the phase function $g(\varphi')$ from Eq. (17) is displayed in this equivalent form:

$$g(\varphi') = A \sin(\varphi' + \Phi)$$

with

$$A = \sqrt{\sin^2\vartheta_i + \sin^2\vartheta_s + 2 \sin\vartheta_i \sin\vartheta_s \cos\chi_0}$$

$$\tan\Phi = \frac{\sin\vartheta_i \cos\varphi_i + \sin\vartheta_s \cos\varphi_s}{\sin\vartheta_i \sin\varphi_i + \sin\vartheta_s \sin\varphi_s} \qquad (22)$$

$$\chi_0 = \varphi_i - \varphi_s .$$

So the diffraction integral (21) can be re-written:

$$I_{e,m}^{s,c;s,c} \approx \delta_{e,m}(\varphi_0') \int_0^{2\pi} \begin{Bmatrix} \sin(\varphi' - \varphi_i) \\ \cos(\varphi' - \varphi_i) \end{Bmatrix} \times \begin{Bmatrix} \sin(\varphi' - \varphi_s) \\ \cos(\varphi' - \varphi_s) \end{Bmatrix} e^{jk_0 aA \sin(\varphi' + \Phi)} d\varphi' .$$

After an elementary transformation of the trigonometric products all eight diffraction integrals can be reduced to three remaining types I_0, I_c and I_s:

$$I_{e,m}^{ss} \approx \delta_{e,m}(\varphi_0') \frac{1}{2} (I_0 \cos\chi_0 - I_c)$$
$$I_{e,m}^{sc} \approx \delta_{e,m}(\varphi_0') \frac{1}{2} (-I_0 \sin\chi_0 + I_s)$$
$$I_{e,m}^{cs} \approx \delta_{e,m}(\varphi_0') \frac{1}{2} (I_0 \sin\chi_0 + I_s)$$
$$I_{e,m}^{cc} \approx \delta_{e,m}(\varphi_0') \frac{1}{2} (I_0 \cos\chi_0 + I_c) .$$

With the abreviations

$$\alpha = k_0 a A \quad \text{and} \quad \tau = \varphi' + \Phi - \frac{\pi}{2}$$

the remaining basic integrals are:

$$I_0 = \int_{\Phi - \frac{\pi}{2}}^{\Phi + \frac{3\pi}{2}} e^{j\alpha \cos\tau}\, d\tau$$

$$I_c = -I_2^c \cos\chi_2 - I_2^s \sin\chi_2$$
$$I_s = I_2^c \sin\chi_2 - I_2^s \cos\chi_2$$

with

$$\chi_2 = 2\Phi + \varphi_i + \varphi_s$$

and

$$I_2^{c,s} = \int_{\Phi - \frac{\pi}{2}}^{\Phi + \frac{3\pi}{2}} \begin{Bmatrix} \cos 2\tau \\ \sin 2\tau \end{Bmatrix} e^{j\alpha \cos\tau}\, d\tau .$$

The integrals I_0, I_2^c and I_2^s are denoted as Sommerfeld's integrals; they can be solved rigorously using the ordinary Bessel functions J_0 and J_2 (*Weyrich* [16]):

$$I_0 = 2\pi J_0(\alpha)$$
$$I_2^c = -2\pi J_2(\alpha)$$
$$I_2^s = 0 .$$

The wanted approximations for the diffraction integrals can now be given using a clear matrix notation:

$$\begin{bmatrix} I_{e,m}^{ss} \\ I_{e,m}^{sc} \\ I_{e,m}^{cs} \\ I_{e,m}^{cc} \end{bmatrix} \approx \pi \delta_{e,m}(\varphi_0') \begin{bmatrix} \cos\chi_0 & -\cos\chi_2 \\ -\sin\chi_0 & -\sin\chi_2 \\ \sin\chi_0 & -\sin\chi_2 \\ \cos\chi_0 & \cos\chi_2 \end{bmatrix} \begin{bmatrix} J_0(\alpha) \\ J_2(\alpha) \end{bmatrix} \qquad (23)$$

with $\chi_0 = \varphi_i - \varphi_s$ and $\chi_2 = 2\Phi + \varphi_i + \varphi_s$, Φ and A from Eq. (22) and $\alpha = k_0 a A$. Together with the Eqs. (14) and (15) and the general values of the modified diffraction coefficients $\delta_{e,m}(\varphi_0')$ at the stationary point, one obtains a closed approximative representation of the scattered far-field. Comparisons of the approximate solution with a numerical Gauss quadratur of the diffraction integrals show a good agreement. In the monostatic special case *Pathak et al* [10] made comparisons with the exact Wiener Hopf solution for the diffraction at a semi-infinite circular cylinder and they found also a good agreement with their approximate solution in the whole range of aspect angles.

5. Far-zone fields

Using the equivalent current method (ECM) a far-zone representation of the field which is bistaticly scattered at the circular edge was given in the Eqs. (14) and (15). Then the eight different diffraction integrals were solved approximately (see Eq. (23)). In the following the scattered field components will be transformed to a formal scattering matrix notation.

5.1 Scattering matrix formulation

The Eqs. (14) and (15) which show the far-zone components of the scattered field can be re-arranged in matrix notation:

$$\begin{pmatrix} E_\vartheta^s \\ E_\varphi^s \end{pmatrix} = [S] \begin{pmatrix} E_\vartheta^i \\ E_\varphi^i \end{pmatrix} \frac{e^{-j k_0 r_s}}{k_0 r_s}$$
$$\begin{pmatrix} H_\vartheta^s \\ H_\varphi^s \end{pmatrix} = Y_0 [V] \begin{pmatrix} E_\vartheta^s \\ E_\varphi^s \end{pmatrix} \tag{24}$$

with the transformation matrix

$$[V] = \begin{pmatrix} 0 & -1 \\ 1 & 0 \end{pmatrix} . \tag{25}$$

The components of the incident wave are taken at the origin ($r = 0$) and they are, according to Eq. (1), identical to the complex phasors A_ϑ^i and A_φ^i:

$$E_\vartheta^i = E_\vartheta^i \big|_{r=0} = A_\vartheta^i$$
$$E_\varphi^i = E_\varphi^i \big|_{r=0} = A_\varphi^i . \tag{26}$$

$[S]$ is the far-zone scattering matrix with the following form:

$$[S] = \begin{pmatrix} S_{\vartheta\vartheta} & S_{\vartheta\varphi} \\ S_{\varphi\vartheta} & S_{\varphi\varphi} \end{pmatrix} \tag{27}$$

and the separate scattering coefficients are:

$$S_{\vartheta\vartheta} = I_e^{ss} \cos\vartheta_i \cos\vartheta_s - I_m^{cc}$$
$$S_{\vartheta\varphi} = -I_e^{cs} \cos\vartheta_s - I_m^{sc} \cos\vartheta_i$$
$$S_{\varphi\vartheta} = -I_e^{sc} \cos\vartheta_i - I_m^{cs} \cos\vartheta_s$$
$$S_{\varphi\varphi} = I_e^{cc} - I_m^{ss} \cos\vartheta_i \cos\vartheta_s .$$

Using following decomposition of the approximate solutions of the diffraction integrals (see Eq. (23))

$$I_{e,m}^{ss} = \delta_{e,m}(\varphi_0')\, I^{ss}$$
$$I_{e,m}^{sc} = \delta_{e,m}(\varphi_0')\, I^{sc}$$
$$I_{e,m}^{cs} = \delta_{e,m}(\varphi_0')\, I^{cs} \tag{28}$$
$$I_{e,m}^{cc} = \delta_{e,m}(\varphi_0')\, I^{cc} ,$$

the scattering matrix $[S]$ for the edge of the aperture can be split up into two separate scattering matrices:

$$[S] = \delta_e(\varphi_0')\,[S_e] + \delta_m(\varphi_0')\,[S_m] \tag{29}$$

with

$$[S_e] = \begin{pmatrix} I^{ss} \cos\vartheta_i \cos\vartheta_s & -I^{cs} \cos\vartheta_s \\ -I^{sc} \cos\vartheta_i & I^{cc} \end{pmatrix}$$

and

$$[S_m] = \begin{pmatrix} -I^{cc} & -I^{sc} \cos\vartheta_i \\ -I^{cs} \cos\vartheta_s & -I^{ss} \cos\vartheta_i \cos\vartheta_s \end{pmatrix} .$$

With the decomposition (29) the scattering contribution excited by the electric equivalent edge current I_e can be investigated separately from the contribution excited by the magnetic equivalent edge current I_m. There exists a remarkable relation between both scattering matrices:

$$[S_m] = [V][S_e][V]$$

using the transformation matrix $[V]$ from Eq. (25).

5.2 Polarization effects

Since the cylindrical scatterer is rotationally symmetrical one only needs to consider the azimuthal angle of incidence $\varphi_i = 0°$ (see Figure 1) without loss of generality. Thus a linear (V-H) polarization basis can be build up very simply:

$$E_V = E_\vartheta , \quad E_H = E_\varphi .$$

So the scattering matrix for linear polarization (vertical or horizontal) is identical to the scattering matrix $[S]$ from Eq. (24). A circular polarization basis (LHC-RHC) can be obtained using the transformation:

$$\begin{pmatrix} E_{LHC} \\ E_{RHC} \end{pmatrix} = [U] \begin{pmatrix} E_V \\ E_H \end{pmatrix}$$

with the unitary matrix

$$[U] = \frac{1}{\sqrt{2}} \begin{pmatrix} 1 & -j \\ 1 & j \end{pmatrix} .$$

The imaginary unit is $j = \sqrt{-1}$. The unitary matrix $[U]$ fulfills the condition $[U]^* = ([U]^{-1})^t$, i.e. the complex conjugate matrix is identical to the transposed of the inverse matrix. Thus for $\varphi_i = 0°$ one can write:

$$\begin{pmatrix} E_\vartheta \\ E_\varphi \end{pmatrix} = [U]^{-1} \begin{pmatrix} E_{LHC} \\ E_{RHC} \end{pmatrix} . \tag{30}$$

Introducing this transformation (30) into the scattering equations (24) leads to the relation between incident and scattered circularly polarized waves:

$$\begin{pmatrix} E_{LHC}^s \\ E_{RHC}^s \end{pmatrix} = [U][S][U]^{-1} \begin{pmatrix} E_{LHC}^i \\ E_{RHC}^i \end{pmatrix} \frac{e^{-j k_0 r_s}}{k_0 r_s} . \tag{31}$$

Just as in Eq. (26) the incident field is taken at the origin $r = 0$. Using the transformation (30) one finds:

$$E_{LHC}^i = \frac{1}{\sqrt{2}} \left(A_\vartheta^i - j A_\varphi^i \right)$$
$$E_{RHC}^i = \frac{1}{\sqrt{2}} \left(A_\vartheta^i + j A_\varphi^i \right) .$$

Starting from the scattering matrix $[S]$ in Eq. (27) which holds for linear polarization vectors, the new polarization matrix $[S_U]$ for a circular polarization basis is obtained after two matrix multiplications:

$$[S_U] = [U][S][U]^{-1} = \begin{pmatrix} S_{LL} & S_{LR} \\ S_{RL} & S_{RR} \end{pmatrix} . \quad (32)$$

The particular scattering coefficients are:

$$\begin{aligned} S_{LL} &= S_{RR}^{*} = \frac{1}{2}[S_{\vartheta\vartheta} + S_{\varphi\varphi} + j(S_{\vartheta\varphi} - S_{\varphi\vartheta})] \\ S_{LR} &= S_{RL}^{*} = \frac{1}{2}[S_{\vartheta\vartheta} - S_{\varphi\varphi} - j(S_{\vartheta\varphi} + S_{\varphi\vartheta})] . \end{aligned} \quad (33)$$

6. Scattering diagrams

To demonstrate the scattering behaviour at the rim of the aperture of a semi-infinite circular cylinder the spatial distribution of the radial energy-flux density of the scattered field is considered:

$$P_{r_s}^{s} = \frac{1}{2} Re\left\{ \vec{E}^{s} \times \left(\vec{H}^{s}\right)^{*} \right\} \cdot \hat{r}_s .$$

Because of the condition $\vec{H}^{s} = Y_0 \hat{r}_s \times \vec{E}^{s}$ the far-zone formula simply reads:

$$P_{r_s}^{s} = \frac{Y_0}{2}\left(|E_{\vartheta}^{s}|^2 + |E_{\varphi}^{s}|^2 \right) .$$

Using the scattering equations (24) the radial energy-flux density in the far-zone can be determined:

$$P_{r_s}^{s} = \frac{Y_0}{2}\left\{ \left| A_{\vartheta}^{i} S_{\vartheta\vartheta} + A_{\varphi}^{i} S_{\vartheta\varphi} \right|^2 + \left| A_{\vartheta}^{i} S_{\varphi\vartheta} + A_{\varphi}^{i} S_{\varphi\varphi} \right|^2 \right\} \frac{1}{(k_0 r_s)^2} .$$

The normalized radiation characteristic C which is commonly displayed in a logarithmic form is then derived:

$$C(\vartheta_i, \vartheta_s, \varphi_i, \varphi_s) = \frac{P_{r_s}^{s}(\vartheta_i, \vartheta_s, \varphi_i, \varphi_s)}{P_{r_s\,\max}^{s}} .$$

$P_{r_s\,\max}^{s}$ is a normalization factor which specifies the energy-flux density in the main radiation direction. Symmetry considerations for the scattering at a circular cylinder indicate that the radiation characteristic does not depend on the azimuthal angle $\varphi_i = \varphi_s$ in the *monostatic* case while in the *bistatic* case only the difference $(\varphi_i - \varphi_s)$ between both angles influences the scattering diagram:

$$\begin{aligned} C^{m} &= C(\vartheta_s) \\ C^{b} &= C(\vartheta_i, \vartheta_s, \varphi_i - \varphi_s) . \end{aligned} \quad (34)$$

A vertically polarized incident wave implies $A_{\varphi}^{i} = 0$ for $\varphi_i = 0°$ and one obtains the non-normalized scattering characteristic C_V:

$$C_V = |S_{\vartheta\vartheta}|^2 + |S_{\varphi\vartheta}|^2 . \quad (35)$$

In an analogous manner is $A_{\vartheta}^{i} = 0$ for an incident horizontally polarized wave and one gets:

$$C_H = |S_{\varphi\varphi}|^2 + |S_{\vartheta\varphi}|^2 . \quad (36)$$

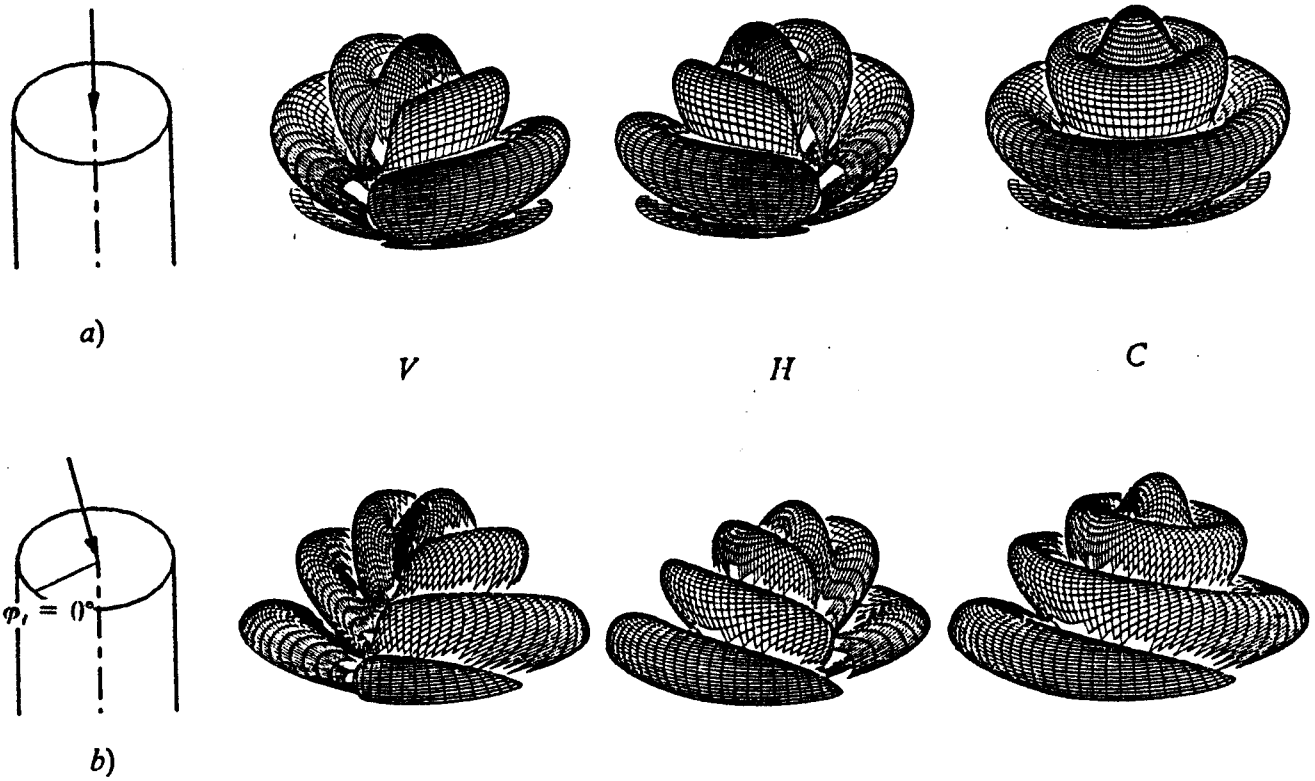

Figure 4. Bistatic radiation characteristic. C_V, C_H and C_C (see the Eqs. (35) to (37)) for an incident vertically, horizontally or circularly polarized plane wave. The diameter $2a$ of the circular cylinder is three wavelengths ($k_0 a = 3\pi$). Two different situations are displayed: a) axial incidence ($\vartheta_i = 0°$) and b) oblique incidence ($\vartheta_i = 15°$).

An incident plane wave with circular polarization yields the non-normalized radiation characteristic using Eq. (31):

$$C_C = C_{LHC} = C_{RHC} = 2\left(|S_{LL}|^2 + |S_{LR}|^2\right) = \\ = C_V + C_H = |S_{\vartheta\vartheta}|^2 + |S_{\varphi\vartheta}|^2 + |S_{\varphi\varphi}|^2 + |S_{\vartheta\varphi}|^2 . \quad (37)$$

For a normalized waveguide radius $k_0 a = 3\pi$ ($2a = 3\lambda_0$) the following three-dimensional polar plots show the spatial distribution of the radial energy-flux density of the scattered field in the bistatic scattering problem. A logarithmic representation with a dynamic range of -40 dB to 0 dB was used. The direction of incidence of the plane wave is indicated by $\varphi_i = 0°$ and $\vartheta_i = 0°$ or $\vartheta_i = 15°$. The scattering diagram is only displayed in the range $0° \leq \vartheta_{i,s} \leq 70°$. For an incident vertically, horizontally or circularly polarized plane wave the corresponding radiation characteristic C_V, C_H and C_C is shown in Figure 4.

7. Concluding remarks

This paper considered the radar problem of bistatic scattering of plane electromagnetic waves at a semi-infinite circular cylinder. The diffraction at the circular rim of the aperture was investigated in detail. To avoid the singularity problem at caustics occuring in ray-optical high frequency solutions the ECM was applied which is based on the geometrical theory of diffraction. The diffraction integrals could be solved approximately to determine the scattered field in the far-zone.

The field of application of the ECM computations is restricted to the domain $0° \leq \vartheta_{i,s} \leq 70°$. An extension to all angles of space including the incident and the reflection shadow boundary is possible using a combination of ECM with UTD; the latter method yields a non-singular field representation in off-caustic regions.

Of special interest is a future investigation of the scattered field in the direct near-zone of the aperture of the waveguide. To improve the precision of the performed approximate computations higher oder terms can be introduced which arise from multiply diffracted rays. Furthermore other waveguide excitations than just a plane wave can be considered. In *Schroth* and *Kark* [14] the excitation by an electric dipole located on the symmetry axis of the circular cylinder can be found.

Bibliography

[1] Erdélyi, A.: *Asymptotic Expansions.* Dover Publ., New York (1956), 51-56.

[2] James, G.L.: *Geometrical Theory of Diffraction for Electromagnetic Waves.* IEE Electromagnetic Waves Series 1, Peregrinus, Stevenage (1976), 28-34.

[3] Johnson, T.W.; Moffat, D.L.: *Electromagnetic Scattering by Open Circular Waveguides.* Radio Science, vol. 17 (1982), 1547-1556.

[4] Kark, K.W.: *Theoretische Untersuchungen zur bistatischen Streuung an einer kreisförmigen Kante.* National U.R.S.I. Conference, F.R. Germany, Proceedings: Kleinheubacher Berichte, vol. 32 (1988).

[5] Keller, J.B.: *Geometrical Theory of Diffraction.* Journal Optical Society Am., vol. JOSA-52 (1962), 116-130.

[6] Knott, E.F.; Senior,T.B.A.: *Equivalent Currents for a Ring Discontinuity.* IEEE Trans. Antennas Propagat., vol. AP-21 (1973), 693-695.

[7] Knott, E.F.; Senior, T.B.A.: *Comparison of Three High-Frequency Diffraction Techniques.* Proc. of the IEEE, vol. 62 (1974), 1468-1474.

[8] Kouyoumjian, R.G.; Pathak, P.H.: *A Uniform Geometrical Theory of Diffraction for an Edge in a Perfectly Conducting Surface.* Proc. of the IEEE, vol. 62 (1974), 1448-1461.

[9] Kouyoumjian, R.G.; Pathak, P.H.; Burnside, W.D.: *A Uniform GTD for the Diffraction by Edges, Vertices and Convex Surfaces; 497-561 in: Skwirzynski, J.K. (Ed.): NATO Advanced Study Institute on Theoretical Methods for Determining the Interaction of Electromagnetic Waves with Structures.* Sijthoff & Noordhoff, Alphen aan den Rijn, The Netherlands, (1981).

[10] Pathak, P.H.; Huang, C.C.; Lai, C.Y.; Moffat, D.L.: *Analysis of Electromagnetic Backscatter from an Inlet Cavity Configuration.* Final Report 712661-4, The Ohio State University, ElectroScience Laboratory, Department of Electrical Engineering (1983), 37-39.

[11] Pathak, P.H.; Chuang, C.W.; Liang, M.C.: *Near Field Scattering by Rectangular and Circular Inlet Configurations.* Final Report 716495-2, The Ohio State University, ElectroScience Laboratory, Department of Electrical Engineering (1985), 20-28.

[12] Pathak, P.H.: *Techniques for High Frequency Problems; Kap.4 (Teil A) in: Lo, Y.T.; Lee, S.W. (Eds.): Handbook of Antenna Theory and Design.* Van Nostrand, New York (1988).

[13] Schroth, A.; Stein, V.: *Moderne numerische Verfahren zur Lösung von Antennen- und Streuproblemen.* Oldenbourg, München (1985), 30-91.

[14] Schroth, A.; Kark, K.W.: *Anwendung der geometrischen Beugungstheorie in der EMV-Analyse.* EMV-Kongreß, Karlsruhe, 18.-20.10.88.

[15] Silver, S.: *Microwave Antenna Theory and Design.* MIT Radiation Laboratory Series, McGraw-Hill (1949), 87-90.

[16] Weyrich, R.: *Die Zylinderfunktionen und ihre Anwendungen.* Teubner, Leipzig (1937), 12-28.